



THE UNIVERSITY *of* EDINBURGH

Edinburgh Research Explorer

A wide planetary-mass companion to a young low-mass brown dwarf in Ophiuchus

Citation for published version:

Fontanive, C, Allers, KN, Pantoja, B, Biller, B, Dubber, S, Zhang, Z, Dupuy, T, Liu, MC & Albert, L 2020, 'A wide planetary-mass companion to a young low-mass brown dwarf in Ophiuchus', *Astrophysical Journal Letters*, vol. 905, no. 2, L14, pp. 1-7. <https://doi.org/10.3847/2041-8213/abcaf8>

Digital Object Identifier (DOI):

[10.3847/2041-8213/abcaf8](https://doi.org/10.3847/2041-8213/abcaf8)

Link:

[Link to publication record in Edinburgh Research Explorer](#)

Document Version:

Peer reviewed version

Published In:

Astrophysical Journal Letters

General rights



Copyright for the publications made accessible via the Edinburgh Research Explorer is retained by the author(s) and / or other copyright owners and it is a condition of accessing these publications that users recognise and abide by the legal requirements associated with these rights.

Take down policy

The University of Edinburgh has made every reasonable effort to ensure that Edinburgh Research Explorer content complies with UK legislation. If you believe that the public display of this file breaches copyright please contact openaccess@ed.ac.uk providing details, and we will remove access to the work immediately and investigate your claim.



A WIDE PLANETARY-MASS COMPANION TO A YOUNG LOW-MASS BROWN DWARF IN OPHIUCHUS

CLÉMENTE FONTANIVE ¹, KATELYN N. ALLERS ², BLAKE PANTOJA,² BETH BILLER ³, SOPHIE DUBBER,³
ZHOUJIAN ZHANG ⁴, TRENT DUPUY ³, MICHAEL C. LIU ⁴, AND LOIČ ALBERT ⁵

¹*Center for Space and Habitability, University of Bern, Gesellschaftsstrasse 6, 3012 Bern, Switzerland*

²*Department of Physics and Astronomy, Bucknell University, Lewisburg, PA 17837, USA*

³*SUPA, Institute for Astronomy, University of Edinburgh, Blackford Hill, Edinburgh EH9 3HJ, UK*

⁴*Institute for Astronomy, University of Hawai'i, 2680 Woodlawn Drive, Honolulu, HI 96822, USA*

⁵*Institut de recherche sur les exoplanètes, Université de Montréal, Montréal, H3C 3J7, Canada*

(Received October 22, 2020; Revised November 6, 2020; Accepted November 17, 2020)

Submitted to ApJL

ABSTRACT

We present the discovery of a planetary-mass companion to CFHTWIR-Oph 98, a low-mass brown dwarf member of the young Ophiuchus star-forming region, with a wide 200-au separation (1''46). The companion was identified using *Hubble Space Telescope* images, and confirmed to share common proper motion with the primary using archival and new ground-based observations. Based on the very low probability of the components being unrelated Ophiuchus members, we conclude that Oph 98 AB forms a binary system. From our multi-band photometry, we constrain the primary to be an M9–L1 dwarf, and the faint companion to have an L2–L6 spectral type. For a median age of 3 Myr for Ophiuchus, fits of evolutionary models to measured luminosities yield masses of $15.4 \pm 0.8 M_{\text{Jup}}$ for Oph 98 A and $7.8 \pm 0.8 M_{\text{Jup}}$ for Oph 98 B, with respective effective temperatures of 2320 ± 40 K and 1800 ± 40 K. For possible system ages of 1–7 Myr, masses could range from 9.6–18.4 M_{Jup} for the primary, and from 4.1–11.6 M_{Jup} for the secondary. The low component masses and very large separation make this binary the lowest binding energy system imaged to date, indicating that the outcome of low-mass star formation can result in such extreme, weakly-bound systems. With such a young age, Oph 98 AB extends the growing population of young free-floating planetary-mass objects, offering a new benchmark to refine formation theories at the lowest masses.

Keywords: binaries: general — brown dwarfs — stars: individual (CFHTWIR-Oph 98)

1. INTRODUCTION

Currently only a handful of planetary-mass companions ($< 13 M_{\text{Jup}}$) are known around young (< 20 Myr) brown dwarfs (Chauvin et al. 2005; Todorov et al. 2010; Béjar et al. 2008; Best et al. 2017; Dupuy et al. 2018). These objects are unlikely to have formed in the disk of their primary, however, they possess similar masses and temperatures as young self-luminous giant exoplanets. This small but growing population of binaries provides critical tests for theoretical models. While the method of their formation differs from that of planets

orbiting stars, the frequency and properties of such systems constrain formation theories of the lowest-mass objects. With well-determined ages compared to field brown dwarfs, each of these binaries also provides an important archetypal system for validating atmosphere and evolutionary models.

The best studied of these companions, 2M1207b (Chauvin et al. 2005), was quite puzzling at the time of its discovery, as it appears to have very red near-infrared colors compared to model predictions given its luminosity (Mohanty et al. 2007). Interestingly, the first directly-imaged exoplanets are similarly red (Marois et al. 2008; Barman et al. 2011). This is attributed to the low surface gravity of young objects and is found as well for free-floating brown dwarfs (e.g. Cruz et al. 2009; Faherty et al. 2009; Liu et al. 2016). Low surface gravity

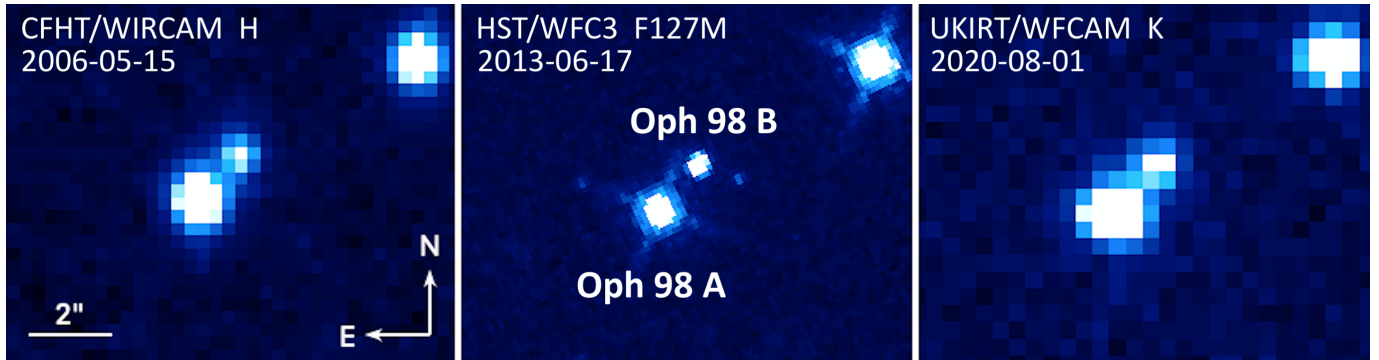


Figure 1. Images of the Oph 98 binary system from the first epoch of CFHT data (left), *HST* observations (middle) and UKIRT data (right). North is up and East is left. The angular scale is indicated in the left panel and is the same for all images. The source North-West of the binary (upper right corner) is the reference background star *Gaia* DR2 6050679111185185664.

has implications for the cloud structure of these benchmark objects – their red colors suggest that they retain dusty silicate clouds down to much lower effective temperatures compared to high surface gravity field brown dwarfs at similar temperatures. Discovering and characterizing even younger planetary-mass objects allows us to study these atmospheres at the very youngest ages and lowest surface gravities.

2M1207b is a member of the ~ 11 -Myr TW Hya association; identifying similar systems at even younger ages enables strong constraints on the formation of such objects (cluster environment, accretion processes, presence of disks), as well as to trace the early evolution of their physical properties. In this Letter, we report the discovery of such a young low-mass binary, CFHTWIR-Oph 98 (hereafter Oph 98; 2MASS J16274422–2358521). The brown dwarf Oph 98 A is a ~ 15 - M_{Jup} member of the ~ 3 -Myr Ophiuchus star-forming region (Alves de Oliveira et al. 2012). Using ground- and space-based observations, we confirm and characterize Oph 98 B as a faint and red co-moving companion with a mass of $\sim 8 M_{\text{Jup}}$, and a large separation of about 200 au.

2. OBSERVATIONS AND DATA ANALYSIS

2.1. Hubble Space Telescope data

We observed Oph 98 as part of a *Hubble Space Telescope* (*HST*) multiplicity survey (GO 12944, PI Allers) targeting brown dwarfs in the Ophiuchus star-forming region. Data for this target were acquired on UT 2013 June 17. Two sets of deep dithered images were obtained in the F127M and F139M filters on the IR channel of the WFC3 instrument, in full frame MULTIACCUM mode, with total exposure times of 698 s in each band. Two images of 473 s each were then acquired in the F850LP bandpass on the UVIS channel, using the full UVIS aperture. The combination of these three filters allows for clear distinctions of sub-stellar objects

from background interlopers, by exploiting the inherent red colors of brown dwarfs and a characteristic water absorption band observed in their spectra at $1.4 \mu\text{m}$ (Fontanive et al. 2018; Allers & Liu 2020). Oph 98 A was indeed found to show distinctive photometric colors between these bands compared to other stars in the *HST* field of view. A faint companion, well resolved in all images and shown in the F127M band in Figure 1 (middle panel), was detected at $\sim 1''.46$ from the known brown dwarf based on its multi-band photometry.

The pipeline processed flat-field images were used as input in the *MultiDrizzle* software (Fruchter & Hook 2002) to correct for geometric distortion, perform cosmic ray rejection and combine all dithered frames into a final image in each filter. Source positions were extracted using the *DAOSStarFinder* algorithm from the *Photutils* python package (Bradley et al. 2019). Aperture photometry was performed adopting $0''.4$ aperture radii. The background level and its uncertainty in each final data frame was estimated by applying the same $0''.4$ aperture to 2000 random star-free positions and computing the mean and standard deviation of these measurements. Measured fluxes were finally converted into Vega magnitudes using the *HST* photometric zero points for $0''.4$ apertures in the considered filters. Measured magnitude differences (Δmag) and relative positions between Oph 98 A and B are reported in Table 1. Apparent *HST* magnitudes are listed in Table 2.

2.2. Canada-France-Hawaii Telescope data

Seeing-limited, broad-band *J*, *H*, and *Ks* (MKO filter system) images of Oph 98 are available from the Canada-France-Hawaii Telescope (CFHT) WIRCAM archive (Programs 06AF01, 06AT08, and 12AT09), with data acquired in May 2006 and August 2012. A CFHT *H*-band image of Oph 98 is shown in left panel of Figure 1.

We used pre-processed images from the CFHT facility pipeline, *Tiwi*, which includes detrending and sky sub-

Table 1. Photometric and astrometric measurements of Oph 98 AB

UT Date	Telescope/Instrument	Filter	Δmag	Separation [mas]	Position Angle [deg]
2006 May 16	CFHT/WIRCAM	<i>J</i>	2.089 ± 0.032	1503.67 ± 19.94	318.0 ± 0.8
2006 May 15	CFHT/WIRCAM	<i>H</i>	1.760 ± 0.055	1451.31 ± 26.4	318.7 ± 1.1
2006 May 16	CFHT/WIRCAM	<i>Ks</i>	1.536 ± 0.020	1478.6 ± 15.11	319.7 ± 0.6
2012 Aug 10	CFHT/WIRCAM	<i>J</i>	2.169 ± 0.077	1478.76 ± 33.47	319.0 ± 1.3
2012 Aug 10	CFHT/WIRCAM	<i>H</i>	1.755 ± 0.033	1485.08 ± 17.78	318.8 ± 0.7
2012 Aug 10	CFHT/WIRCAM	<i>Ks</i>	1.630 ± 0.021	1443.32 ± 14.99	319.6 ± 0.6
2013 Jun 17	<i>HST</i> /WFC3	F850LP	2.783 ± 0.171	1458.04 ± 1.54	318.8 ± 0.1
2013 Jun 17	<i>HST</i> /WFC3	F127M	2.192 ± 0.014	1458.19 ± 6.94	319.1 ± 0.3
2013 Jun 17	<i>HST</i> /WFC3	F139M	2.032 ± 0.017	1460.55 ± 6.46	319.2 ± 0.3
2020 Aug 01	UKIRT/WFCAM	<i>J</i>	2.073 ± 0.028	1462.58 ± 20.21	316.7 ± 0.8
2020 Aug 01	UKIRT/WFCAM	<i>K</i>	1.642 ± 0.039	1435.07 ± 8.49	322.0 ± 0.4
2020 Sep 17	UKIRT/WFCAM	<i>H</i>	1.793 ± 0.025	1519.51 ± 21.57	319.0 ± 0.8

traction. We determined the relative astrometry and photometry of Oph 98 A and B from individual pre-processed frames. We used the IDL Astronomy Library’s FIND, APER, and GETPSF routines (Landsman 1993) to determine the point spread function (PSF) and residuals for non-saturated stars within 1 arcmin of Oph 98 A. Using the NSTAR program, we fit the PSF to Oph 98 A, and subtracted it from the image using SUBSTAR. We then fit a model PSF to Oph 98 B. For each epoch and each filter, we determined the separation, position angle, and Δmag of the binary using the mean and standard deviation of the mean of measurements from individual (non-stacked) frames. Table 1 reports our measurements.

We also determined MKO photometry of Oph 98 A and B from the individual, pre-processed frames. We used the magnitudes calculated by NSTAR during the PSF fitting process, and determined the photometric calibration offset for each image by comparing the PSF-fit magnitudes of non-saturated stars within 1 arcmin of Oph 98 A to their 2MASS photometry. We first converted their 2MASS magnitudes to the MKO system using custom color corrections derived from synthetic photometry of SpeX Spectral Library spectra reddened by A_V of 1–30 mag. We calculated the photometry for Oph 98 A and B using a weighted mean and weighted standard deviation of the mean of the magnitudes calculated from each frame. Our photometry (Table 2) is in good agreement with published WIRCAM photometry of Oph 98 A from Alves de Oliveira et al. (2012).

2.3. United Kingdom Infra-Red Telescope data

We obtained seeing-limited *J* and *K*-band images of Oph 98 using the United Kingdom Infra-Red Telescope (UKIRT) WFCAM instrument on UT 2020 August 01, followed by an *H*-band dataset on UT 2020 September 17 (Project ID U/20A/H02). The *K*-band image is

shown in Figure 1 (right panel). Using the same procedure described in § 2.2, we determined the photometric and astrometric measurements of Oph 98 AB from individual, pre-processed images, reported in Tables 1 and 2.

3. CHARACTERIZATION OF THE BINARY

3.1. Astrometric Analysis

The relative astrometry of the binary was measured in the various imaging data sets available as detailed in § 2 (Table 1). The left panel of Figure 2 clearly demonstrates that Oph 98 A and B are co-moving over the 14-year time baseline of ground- and space-based data, indicating that the two components share a common proper motion. Based on their coordinates, Oph 98 A and B are most likely part of the young L1688 cloud in the Ophiuchus complex (Esplin & Luhman 2020). Given the stellar density of L1688 (King et al. 2012), the chance of alignment for two unrelated Ophiuchus members within $2''$ is $< 10^{-4}$. This number is an overestimate in the case of such rare low-mass brown dwarfs at the bottom of the initial mass function (Kroupa et al. 2013), and we conclude that Oph 98 A and B form a physically-associated binary pair.

A nearby star (*Gaia* DR2 6050679111185185664), $\sim 6''$ North-West from Oph 98, was found to be in the *Gaia* Data Release 2 (DR2) catalog (Gaia Collaboration et al. 2016, 2018) with a full astrometric solution. With *Gaia* parallax and proper motion measurements of $\varpi = 1.453 \pm 0.641$ mas, $\mu_{\alpha*} = -0.795 \pm 1.396$ mas yr $^{-1}$ and $\mu_{\delta} = -1.192 \pm 0.824$ mas yr $^{-1}$, this source is essentially consistent with a stationary background star. As shown in the right panel of Figure 2, the positions of the star relative to Oph 98 A at each observational epoch are in excellent agreement with the expected relative displacement over time for a background star (black line). The small positional disparities are consistent with the almost negligible motion of the *Gaia* source and with the

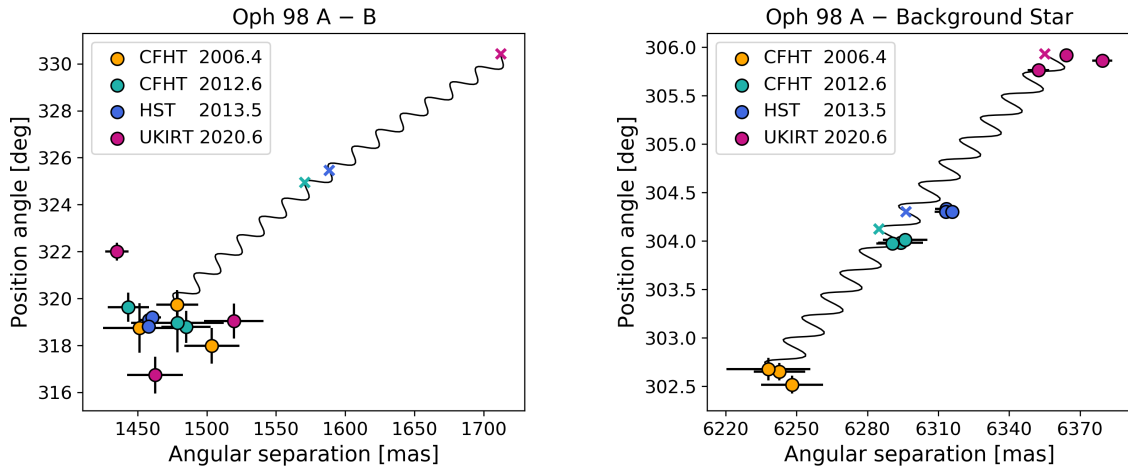


Figure 2. Positions of Oph 98 B (left) and the nearby star *Gaia* DR2 6050679111185185664 (right) relative to Oph 98 A. Measurements are indicated by filled circles, color-coded by observational epoch. The solid black lines show the expected motion of a stationary background star relative to the primary past the first observational epoch, given the parallax and proper motion of Ophiuchus (Table 2). Crosses mark the expected positions of a background source at the given color-coded dates. Oph 98 B is clearly co-moving with Oph 98 A, while the relative motion of the *Gaia* star is fully consistent with a background source.

measurement uncertainties in the original epoch from which the background track is calculated. These results confirm that the primary has a proper motion expected for Ophiuchus, hence validating the Ophiuchus membership of the co-moving Oph 98 AB system.

We adopt the parallax of $\varpi = 7.29 \pm 0.22$ mas derived by Ortiz-León et al. (2018) for the embedded L1688 population based on *Gaia* DR2, in good agreement with values from Cánovas et al. (2019) and Esplin & Luhman (2020). At a corresponding distance of 137 ± 4 pc, the observed angular separation of the Oph 98 binary ($1''.46 \pm 0''.01$) implies a wide projected separation of 200 ± 6 au.

3.2. Photometric Estimates of Spectral Types

In order to estimate the spectral types of Oph 98 A and B, we used the SpeX Prism Library Analysis Toolkit (SPLAT; Burgasser et al. 2016) to fit the spectral energy distribution (SED) of the binary components. We gathered a library of M and L spectra from the SPLAT database, for which we obtained homogeneous near-infrared spectral types and gravity scores using the Allers & Liu (2013) classification, and retained only young sources with very-low (VL-G) gravity scores.

SPLAT allows for the determination of photometric magnitudes on specific filters based on a source’s spectrum. The module can also redden a spectrum following the Cardelli et al. (1989) reddening law. We used these capabilities to determine the scaling factor and visual extinction A_V minimizing the χ^2 between the synthetic photometry of the templates and our measured magnitudes for Oph 98 A and B. We added uncertainties of 0.011, 0.007 and 0.007 mag (2MASS calibration uncer-

tainties; Cutri et al. 2003) to the *JHK* MKO measurements tied to 2MASS, and 2% and 5% uncertainties in the *HST* IR and UVIS photometry¹, respectively.

We observed a strong degeneracy between spectral type and extinction in our results, consistent with findings by Luhman et al. (2017) for young reddened L dwarfs. Results for Oph 98 A showed a handful of fits with similar χ^2 values for objects with spectral types of M9 to L1, and decreasing reddening values with later type over the range $A_V \sim 4$ –6 mag. A similar effect was seen in the results of Oph 98 B, but spanning wider ranges of spectral types (late-M to mid-L) and extinctions ($A_V \sim 4$ –10 mag), likely due to the atypical colors and larger uncertainties on the photometry of the secondary. Assuming the same local cloud extinction for the two components, we can reduce this range to best-fit results yielding $A_V < 6$ mag for the companion. This provides spectral type estimates of M9–L1 for Oph 98 A, and L2–L6 for Oph 98 B, with a visual extinction for the system of $A_V = 5 \pm 1$ mag, placing the primary at the M/L transition and loosely constraining the secondary to be along the L spectral sequence. Our derived quantities for the primary are in reasonable agreement with the values of M9.75 and $A_V = 3$ mag estimated by Alves de Oliveira et al. (2012) from low-resolution *H*- and *K*-band spectroscopy. Additional spectroscopic observations will be required to further characterize the system and break down the observed degeneracies.

¹ <https://www.stsci.edu/hst/instrumentation/wfc3/data-analysis/photometric-calibration>

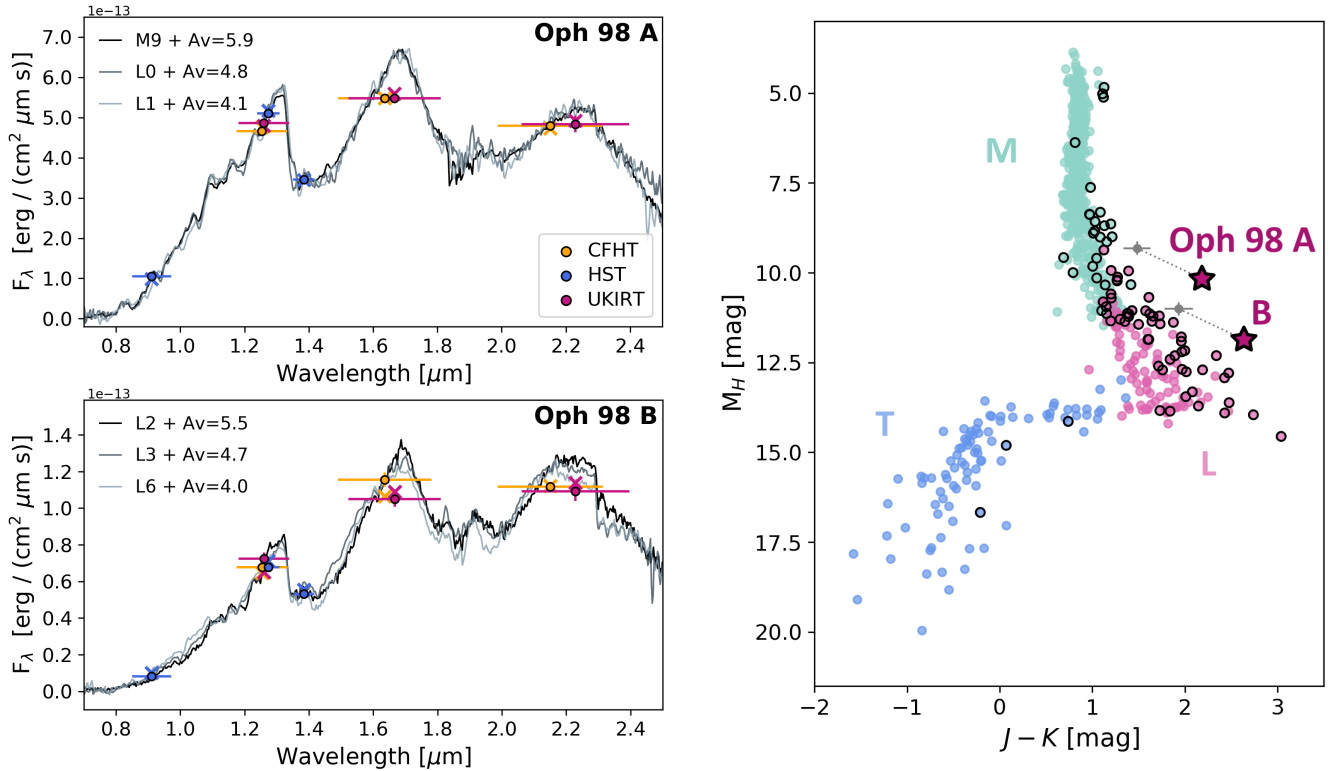


Figure 3. **Left:** SED fits of Oph 98 A (top) and B (bottom). Photometric measurements (filled circles) are compared to a selection of best-fit templates, reddened by their fitted extinctions: TWA 26 (M9 VL-G), PSO J078.9904+31.0171 (L0 VL-G), 2MASS J16410015+1335591 (L1 VL-G), 2MASSW J2206450–421721 (L2 VL-G), 2MASSW J0030300–145033 (L3 VL-G), SDSSp J010752.33+004156.1 (L6 VL-G). Crosses show the synthetic photometry in each band for the L0 and L3 spectra. **Right:** Near-infrared color-magnitude diagram of MLT objects showing H -band absolute magnitudes against $J-K$ colors. The observed WFCAM photometry of Oph 98 AB is plotted in the magenta stars, connected by the dotted lines to extinction-corrected values for $A_V = 5 \pm 1$ mag (grey dots). Objects with black circles are young, low-gravity objects and directly-imaged young companions.

The left panel of Figure 3 shows best-fit template spectra for both components compared to our photometric measurements. The right panel shows the observed positions of Oph 98 A and B (magenta stars) in the near-infrared color-magnitude diagram compared to the population of low-mass stars and brown dwarfs. M dwarfs come from Winters et al. (2015). Late-M, L and T dwarfs are compiled from Dupuy & Liu (2012), Dupuy & Kraus (2013) and Liu et al. (2016). Bold circles represent young objects and companions with low surface gravities, which extend the standard M and L sequences to redder $J-K$ colors. The grey dots connected to Oph 98 A and B indicate the extinction-corrected locations of the binary for our derived extinction value. However, since the reddening is determined by best fits to templates, the dereddened colors may not be representative of the intrinsic colors of the components.

3.3. Physical Properties

Since the age of Ophiuchus can be inferred from stellar members of the region, the luminosities of Oph 98 A and B can provide estimates of the physical properties of

the binary using evolutionary models. Recently, Esplin & Luhman (2020) analyzed the ages of various populations within the Ophiuchus star-forming complex. They estimated ages of ~ 2 and $\sim 3-4$ Myr for embedded and low-extinction members of L1688, respectively. Our estimated extinction for Oph 98 ($A_V = 5 \pm 1$ mag) falls on the boundary of A_V between the two L1688 populations defined by Esplin & Luhman (2020). Thus, we adopt an age of 3 Myr for Oph 98, but ages of 1–7 Myr fall within the interquartile age ranges of L1688.

We calculated the luminosities of Oph 98 A and B using extinction-corrected MKO K_s photometry, the K -band bolometric corrections for young brown dwarfs from Filippazzo et al. (2015), and a parallax for L1688 of 7.29 ± 0.22 mas (Ortiz-León et al. 2018). We used a Monte Carlo approach to determine uncertainties, taking a uniform distribution of A_V and spectral type, and normally-distributed uncertainties for the bolometric corrections and parallax. We determine luminosities of $\log(L_{\text{bol}}/L_\odot) = -2.85 \pm 0.06$ dex and -3.49 ± 0.06 dex for Oph 98 A and B, respectively.

Table 2. Properties of the CFHTWIR-Oph 98 AB system

Parameter	Oph 98 A	Oph 98 B	Reference
ASTROMETRY			
α (ICRS J2000.0)	16 ^h 27 ^m 44 ^s .226		Cutri et al. (2003)
δ (ICRS J2000.0)	−23°58′52″.14		Cutri et al. (2003)
$\mu_{\alpha*}$ [mas yr ^{−1}]	−7.2 ± 2.0		Cánovas et al. (2019)
μ_{δ} [mas yr ^{−1}]	−25.5 ± 1.7		Cánovas et al. (2019)
Parallax [mas]	7.29 ± 0.22		Ortiz-León et al. (2018)
Distance [pc]	137 ± 4		Ortiz-León et al. (2018)
PHOTOMETRY			
2MASS <i>J</i> [mag]	16.775 ± 0.176		Cutri et al. (2003)
2MASS <i>H</i> [mag]	15.574 ± 0.109		Cutri et al. (2003)
2MASS <i>Ks</i> [mag]	14.593 ± 0.098		Cutri et al. (2003)
F850LP [mag]	19.696 ± 0.018	22.479 ± 0.170	This paper
F127M [mag]	16.835 ± 0.005	19.027 ± 0.013	This paper
F139M [mag]	16.959 ± 0.005	18.991 ± 0.016	This paper
WIRCAM <i>J</i> [mag]	17.015 ± 0.016	19.109 ± 0.050	This paper
WIRCAM <i>H</i> [mag]	15.851 ± 0.016	17.541 ± 0.030	This paper
WIRCAM <i>Ks</i> [mag]	14.917 ± 0.009	16.498 ± 0.017	This paper
WFCAM <i>J</i> [mag]	16.975 ± 0.009	19.042 ± 0.038	This paper
WFCAM <i>H</i> [mag]	15.826 ± 0.013	17.620 ± 0.037	This paper
WFCAM <i>K</i> [mag]	14.792 ± 0.039	16.408 ± 0.047	This paper
FUNDAMENTAL PROPERTIES			
A_V [mag]	5 ± 1		This paper
Spectral type [†]	M9–L1	L2–L6	This paper
log(L_{bol}/L_{\odot}) [dex]	−2.85 ± 0.06	−3.49 ± 0.06	This paper
1 Myr			
T_{eff} [K]	2210 ± 60	1740 ± 40	This paper
log g [dex]	3.566 ^{+0.040} _{−0.048}	3.436 ^{+0.010} _{−0.015}	This paper
Radius [R_{Jup}]	2.61 ± 0.05	2.00 ^{+0.04} _{−0.03}	This paper
Mass [M_{Jup}]	9.6 ± 1.4	4.1 ^{+0.4} _{−0.3}	This paper
3 Myr			
T_{eff} [K]	2320 ± 40	1800 ± 40	This paper
log g [dex]	3.845 ^{+0.007} _{−0.008}	3.748 ^{+0.015} _{−0.016}	This paper
Radius [R_{Jup}]	2.38 ^{+0.07} _{−0.08}	1.86 ± 0.05	This paper
Mass [M_{Jup}]	15.4 ± 0.8	7.8 ^{+0.7} _{−0.8}	This paper
7 Myr			
T_{eff} [K]	2370 ± 40	1850 ⁺⁵⁰ _{−40}	This paper
log g [dex]	3.974 ^{+0.010} _{−0.008}	3.984 ^{+0.002} _{−0.009}	This paper
Radius [R_{Jup}]	2.27 ± 0.07	1.77 ^{+0.03} _{−0.05}	This paper
Mass [M_{Jup}]	18.4 ^{+0.8} _{−0.7}	11.6 ^{+0.4} _{−0.8}	This paper
BINARY CHARACTERISTICS			
Separation [arcsec]	1.46 ± 0.01		This paper
Separation [au]	200 ± 6		This paper
Orbital period [yr]*	22 000 ± 1 300		This paper
Mass ratio*	0.509 ^{+0.017} _{−0.023}		This paper
E_b [10^{39} erg]*	8.8 ± 1.4		This paper

[†]Photometric estimates based on near-infrared vL-G spectral templates.

*Quantities calculated for a median age of 3 Myr.

Table 2 presents the masses, effective temperatures (T_{eff}), radii, and surface gravities ($\log g$) of Oph 98 A and B calculated from the DUSTY model isochrones of Chabrier et al. (2000) at ages of 1, 3 and 7 Myr. We estimate parameters for the bounds of the interquartile age range as the underlying age distribution of L1688 is unknown. Comparison of the luminosities to evolutionary models at the adopted age of 3 Myr yields masses of 15.4 ± 0.8 and $7.8^{+0.7}_{-0.8} M_{\text{Jup}}$ for Oph 98 A and B, respectively. Over the possible ages of the system (1–7 Myr), the mass of Oph 98 A could range from 9.6 to 18.4 M_{Jup} , and the mass of Oph 98 B from 4.1 to 11.6 M_{Jup} . The primary mass could therefore lie on either side of the planet/brown dwarf boundary ($\sim 13 M_{\text{Jup}}$), while the secondary is confidently in the planetary-mass regime for all plausible system ages. Calculated masses using the evolutionary models of Saumon & Marley (2008) ($f_{\text{sed}} = 2$) and Burrows et al. (1997) were found to agree with the DUSTY results to within the uncertainties.

From the model-derived masses at 3 Myr and measured angular separation, we also computed the binary mass ratio, orbital period and gravitational binding energy of the system, reported in Table 2. We used a median correction factor of 1.1 from projected separation to true semi-major axis (Dupuy & Liu 2011).

4. DISCUSSION AND CONCLUSIONS

4.1. Comparison to Other Systems

With a primary mass near the deuterium-burning limit (~ 11 – $16 M_{\text{Jup}}$ depending on metallicity; Spiegel et al. 2011) and a companion inside the planetary mass range, Oph 98 AB is among the lowest-mass binaries known to date. Only a handful of systems potentially made of two planetary-mass components have been discovered so far: the TW Hya candidate member 2MASS J1119–1137 (Best et al. 2017), the WISE J1355–8258 spectral binary candidate in the AB Dor moving group (Theissen et al. 2020), and the old field systems WISE J0146+4234 (Dupuy et al. 2015) and CFBDSIR J1458+1013 (Liu et al. 2011) that may be more massive depending on their ages.

Oph 98 is distinct from these binaries in three important aspects: the system’s age, mass ratio and separation. The extremely young age of Ophiuchus makes Oph 98 the youngest system currently known with both components near or below the deuterium burning mass boundary, and is thus the only example of such a binary detected right after birth. Additionally, most of these planetary-mass binaries are in nearly equal-mass configurations. In contrast, Oph 98 has a significantly lower mass ratio ($q = 0.509^{+0.017}_{-0.023}$) for a comparable total mass. Finally, all the systems listed above have very

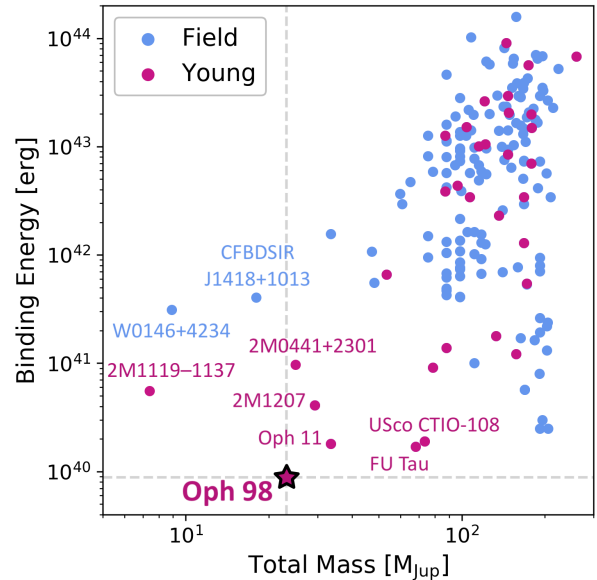


Figure 4. Binding energy plotted against total system mass for low-mass binaries in the field (blue) and young associations (magenta), based on the compilation from Faherty et al. (2020). Oph 98 (magenta star) is among the lowest mass binaries currently known (vertical line) and has the weakest binding energy of any known system (horizontal line).

tight orbital separations (< 5 au), while Oph 98 AB is on a considerably wider 200-au orbit. No old field binaries are known on such large separations in this mass regime (see Fontanive et al. 2018).

In these aspects, Oph 98 is more akin to wide systems with very low-mass companions identified in young associations (≤ 10 Myr). The closest analog to Oph 98 is certainly the other Ophiuchus brown dwarf binary, Oph 11 (17+14 M_{Jup} , 240 au; Close et al. 2007). Lower mass ratio counterparts include 2M1207 (Chauvin et al. 2005) and 2MASS J0441+2301 (Todorov et al. 2010), with ~ 20 - M_{Jup} primaries and planetary-mass secondaries (4–5 M_{Jup}), but significantly shorter separations of a few tens of au; or FU Tau (Luhman et al. 2009) and USco CTIO-108 (Béjar et al. 2008), on separations of hundreds of au, but considerably higher-mass primaries ($\sim 50 M_{\text{Jup}}$) and secondaries around 15 M_{Jup} .

The combination for Oph 98 AB of small estimated component masses ($15.4+7.8 M_{\text{Jup}}$) and large measured separation (200 au) results in a remarkably low binding energy of $E_b = 8.8 \times 10^{39}$ erg. This is lower by a factor of at least 2 than any of the binaries mentioned above, as illustrated in Figure 4, with a second weakest binding energy belonging to FU Tau (see compilation in Faherty et al. 2020). The Oph 98 system is therefore the brown dwarf binary with the lowest gravitational binding energy discovered to date.

4.2. Formation Mechanisms

Oph 98, like each of the young low-mass binaries mentioned in § 4.1, provides a valuable example of a young system in an extreme configuration, offering key insight into formation for the very lowest-mass brown dwarfs. Indeed, as multiplicity is a direct outcome of formation, the properties of very young binaries can serve as key diagnostics of formation pathways. The youth of the Oph 98 system indicates that the involved mechanisms must operate on short Myr-level timescales, compatible with the rapid formation expected from the fragmentation of cloud cores or gravitational instability in disks. The weakly-bound nature of the system argues against violent dynamical processes that would have disrupted the binary, like the premature ejection of substellar embryos from the natal cloud (Reipurth & Clarke 2001). Likewise, formation and subsequent ejection of both components from the disk of a more massive star (Stamatellos et al. 2007) seems implausible based on the binary configuration.

It is more probable that Oph 98 A formed in a star-like manner, through the fragmentation of molecular cloud cores (Whitworth et al. 2007). The low-mass companion Oph 98 B could have formed in the same way, or in the disk of the primary. The latter scenario is unlikely given the mass of the primary, too low to host a disk more massive than $\sim 1 M_{\text{Jup}}$, and the wide binary separation, compared to radii of $< 30\text{--}100$ au for brown dwarf disks (Testi et al. 2016). The mass ratio of ~ 0.5 also suggests a binary-like architecture rather than a planet-like origin for the secondary (Lodato et al. 2005), further supporting the hypothesis that Oph 98 AB emerged from a stellar formation process.

With a lower mass limit for brown dwarfs around $\sim 3 M_{\text{Jup}}$ in a star formation framework (Whitworth et al. 2007) – the minimum mass for opacity-limited fragmentation in turbulent cloud cores (Silk 1977) – Oph 98 B thus extends the growing number of very young, planetary-mass objects populating the low-end tail of the star formation product (e.g. Liu et al. 2013;

Gagné et al. 2014, 2015; Schneider et al. 2016). The existence of such wide, very low-mass binaries arising from a stellar formation pathway is predicted in numerical simulations (Bate 2012), although expected to be of rare occurrence. As the binary with the weakest gravitational binding energy discovered to date, the Oph 98 system therefore represents an unmatched example of the extreme multiplicity outcome of stellar formation.

ACKNOWLEDGMENTS

We thank the anonymous referee for a thorough and constructive report. C.F. acknowledges financial support from the Center for Space and Habitability (CSH). This work has been carried out within the framework of the NCCR PlanetS supported by the Swiss National Science Foundation. Based on observations made with the NASA/ESA Hubble Space Telescope, which is operated by the Association of Universities for Research in Astronomy, Inc., under NASA contract NAS5-26555. These observations are associated with program #12944. Support for this work was provided by NASA through grant numbers 12944, 14686, and 15201 from the Space Telescope Science Institute. This research has been funded in part by grants from the Gordon and Betty Moore Foundation (grant GBMF8550) and the National Science Foundation (AST-1518339) awarded to M. Liu. Based on observations obtained with WIRCam, a joint project of CFHT, Taiwan, Korea, Canada, France, at the Canada-France-Hawaii Telescope (CFHT) which is operated by the National Research Council (NRC) of Canada, the Institut National des Sciences de l’Univers of the Centre National de la Recherche Scientifique of France, and the University of Hawaii. This research has benefited from the SpeX Prism Spectral Libraries, maintained by Adam Burgasser at <http://pono.ucsd.edu/~adam/browndwarfs/spexprism/>. This work made use of the Database of Ultracool Parallaxes maintained by Trent Dupuy at http://www.as.utexas.edu/~tdupuy/plx/Database_of_Ultracool_Parallaxes.html.

REFERENCES

- Allers, K. N., & Liu, M. C. 2013, *ApJ*, 772, 79
 —. 2020, *PASP*, 132, 104401
 Alves de Oliveira, C., Moraux, E., Bouvier, J., & Bouy, H. 2012, *A&A*, 539, A151
 Barman, T. S., Macintosh, B., Konopacky, Q. M., & Marois, C. 2011, *ApJL*, 735, L39
 Bate, M. R. 2012, *MNRAS*, 419, 3115
 Béjar, V. J. S., Zapatero Osorio, M. R., Pérez-Garrido, A., et al. 2008, *ApJL*, 673, L185
 Best, W. M. J., Liu, M. C., Dupuy, T. J., & Magnier, E. A. 2017, *ApJL*, 843, L4
 Bradley, L., Sipőcz, B., Robitaille, T., et al. 2019, *astropy/photutils*: v0.6
 Burgasser, A. J., Aganze, C., Escala, I., et al. 2016, in *American Astronomical Society Meeting Abstracts #227*, Vol. 227, 434.08
 Burrows, A., Marley, M., Hubbard, W. B., et al. 1997, *ApJ*, 491, 856

- Cánovas, H., Cantero, C., Cieza, L., et al. 2019, *A&A*, 626, A80
- Cardelli, J. A., Clayton, G. C., & Mathis, J. S. 1989, *ApJ*, 345, 245
- Chabrier, G., Baraffe, I., Allard, F., & Hauschildt, P. 2000, *ApJ*, 542, 464
- Chauvin, G., Lagrange, A. M., Dumas, C., et al. 2005, *A&A*, 438, L25
- Close, L. M., Zuckerman, B., Song, I., et al. 2007, *ApJ*, 660, 1492
- Cruz, K. L., Kirkpatrick, J. D., & Burgasser, A. J. 2009, *AJ*, 137, 3345
- Cutri, R. M., Skrutskie, M. F., van Dyk, S., et al. 2003, *VizieR Online Data Catalog*, II/246
- Dupuy, T. J., & Kraus, A. L. 2013, *Science*, 341, 1492
- Dupuy, T. J., & Liu, M. C. 2011, *ApJ*, 733, 122
- . 2012, *ApJS*, 201, 19
- Dupuy, T. J., Liu, M. C., & Leggett, S. K. 2015, *ApJ*, 803, 102
- Dupuy, T. J., Liu, M. C., Allers, K. N., et al. 2018, *AJ*, 156, 57
- Esplin, T. L., & Luhman, K. L. 2020, *AJ*, 159, 282
- Faherty, J. K., Burgasser, A. J., Cruz, K. L., et al. 2009, *AJ*, 137, 1
- Faherty, J. K., Goodman, S., Caselden, D., et al. 2020, *ApJ*, 889, 176
- Filippazzo, J. C., Rice, E. L., Faherty, J., et al. 2015, *ApJ*, 810, 158
- Fontanive, C., Biller, B., Bonavita, M., & Allers, K. 2018, *MNRAS*, 479, 2702
- Fruchter, A. S., & Hook, R. N. 2002, *PASP*, 114, 144
- Gagné, J., Lafrenière, D., Doyon, R., Malo, L., & Artigau, É. 2014, *ApJ*, 783, 121
- Gagné, J., Faherty, J. K., Cruz, K. L., et al. 2015, *ApJS*, 219, 33
- Gaia Collaboration, Prusti, T., de Bruijne, J. H. J., et al. 2016, *A&A*, 595, A1
- Gaia Collaboration, Brown, A. G. A., Vallenari, A., et al. 2018, *A&A*, 616, A1
- King, R. R., Parker, R. J., Patience, J., & Goodwin, S. P. 2012, *MNRAS*, 421, 2025
- Kroupa, P., Weidner, C., Pflamm-Altenburg, J., et al. 2013, *The Stellar and Sub-Stellar Initial Mass Function of Simple and Composite Populations*, Vol. 5 (Springer Science), 115
- Landsman, W. B. 1993, in *Astronomical Society of the Pacific Conference Series*, Vol. 52, *Astronomical Data Analysis Software and Systems II*, ed. R. J. Hanisch, R. J. V. Brissenden, & J. Barnes, 246
- Liu, M. C., Dupuy, T. J., & Allers, K. N. 2016, *ApJ*, 833, 96
- Liu, M. C., Delorme, P., Dupuy, T. J., et al. 2011, *ApJ*, 740, 108
- Liu, M. C., Magnier, E. A., Deacon, N. R., et al. 2013, *ApJL*, 777, L20
- Lodato, G., Delgado-Donate, E., & Clarke, C. J. 2005, *MNRAS*, 364, L91
- Luhman, K. L., Mamajek, E. E., Allen, P. R., Muench, A. A., & Finkbeiner, D. P. 2009, *ApJ*, 691, 1265
- Luhman, K. L., Mamajek, E. E., Shukla, S. J., & Loutrel, N. P. 2017, *AJ*, 153, 46
- Marois, C., Macintosh, B., Barman, T., et al. 2008, *Science*, 322, 1348
- Mohanty, S., Jayawardhana, R., Huélamo, N., & Mamajek, E. 2007, *ApJ*, 657, 1064
- Ortiz-León, G. N., Loinard, L., Dzib, S. A., et al. 2018, *ApJL*, 869, L33
- Reipurth, B., & Clarke, C. 2001, *AJ*, 122, 432
- Saumon, D., & Marley, M. S. 2008, *ApJ*, 689, 1327
- Schneider, A. C., Windsor, J., Cushing, M. C., Kirkpatrick, J. D., & Wright, E. L. 2016, *ApJL*, 822, L1
- Silk, J. 1977, *ApJ*, 214, 152
- Spiegel, D. S., Burrows, A., & Milsom, J. A. 2011, *ApJ*, 727, 57
- Stamatellos, D., Hubber, D. A., & Whitworth, A. P. 2007, *MNRAS*, 382, L30
- Testi, L., Natta, A., Scholz, A., et al. 2016, *A&A*, 593, A111
- Theissen, C. A., Bardalez Gagliuffi, D. C., Faherty, J. K., Gagné, J., & Burgasser, A. 2020, *Research Notes of the American Astronomical Society*, 4, 67
- Todorov, K., Luhman, K. L., & McLeod, K. K. 2010, *ApJL*, 714, L84
- Whitworth, A., Bate, M. R., Nordlund, Å., Reipurth, B., & Zinnecker, H. 2007, in *Protostars and Planets V*, ed. B. Reipurth, D. Jewitt, & K. Keil, 459
- Winters, J. G., Henry, T. J., Lurie, J. C., et al. 2015, *AJ*, 149, 5